Int. J. Environ. Sci. Technol. (2016) 13:2579–2596
DOI 10.1007/s13762-016-1094-0

ORIGINAL PAPER

Groundwater flow and residence time in a karst aquifer using ion and isotope characterization

M. A. Díaz-Puga[1] · A. Vallejos[1] · F. Sola[1] · L. Daniele[2,3] · L. Molina[1] · A. Pulido-Bosch[1]

Received: 11 January 2016 / Revised: 4 July 2016 / Accepted: 17 August 2016 / Published online: 7 September 2016

Abstract In order to identify the origin of the main processes that affect the composition of groundwater in a karstic aquifer, a hydrogeochemical and isotopic study was carried out of water from numerous observation wells located in Sierra de Gador, a semiarid region in SE Spain. Several natural and anthropogenic tracers were used to calculate groundwater residence time within this complex aquifer system. Analysis of major ions enabled the principal geochemical processes occurring in the aquifer to be established, and the samples were classified into four distinctive solute groups according to this criterion. Dissolution of carbonate rocks determines the chemical composition of less mineralized water. In another group, the concurrent dissolution of dolomite and precipitation of calcite in gypsum-bearing carbonate aquifer, where the dissolution of relatively soluble gypsum controls the reaction, are the dominant processes. Marine intrusion results in highly mineralized waters and leads to base exchange reactions. The groundwater enrichment of minor and trace elements allowed classification of the samples into two classes that are linked to different flow patterns. One of these classes is influenced by a slow and/or deep regional flow, where the temperature is generally elevated. The influence of sulphate reduces by up to 40 % the barium concentration due to the barite precipitation. Isotope data (T, ^{14}C) confirm the existence of recent local flows, and regional flow system, and ages of ground water may reach 8000 years. The importance of gypsum dissolution in this aquifer is proved by the $\delta^{34}S$ content.

Keywords Karst · Hydrogeochemistry · Minor ions · Isotopes · Groundwater age

Introduction

Karstic carbonate massifs are complex aquifer mediums, in which the circulation of recharge water occurs via fractures, fissures, stratification and/or dissolution surfaces on the rock. Along the flowpath, the chemistry of the water is modified as a function of the materials it traverses due to the water–rock interaction (Moral et al. 2008; Wu et al. 2009). Carbonate aquifers are particularly important in semiarid, densely populated regions such as in the Mediterranean Basin, where they can account for 50 % of the water resources that supply its population (Margat 2008; Caetano Bicalho et al. 2012). Overexploitation of groundwater can lead to a change in its hydrogeochemical characteristics, generally leading to a deterioration in water quality due to processes such as salinization through dissolution of evaporites (Reynauld et al. 1999; Martos-Rosillo and Moral 2015; Vallejos et al. 2015a), or marine intrusion processes (Terzić et al. 2008; Sdao et al. 2012).

The carbonate massif of Sierra de Gador comprises the principal recharge area for the aquifer that has developed beneath this mountain range, as well as for the whole of its southern extension, which lies beneath the coastal plain of Campo de Dalias. The latter represents one of the main

Editorial responsibility: J. Trögl.

✉ A. Vallejos
avallejo@ual.es

[1] Department of Hydrogeology, University of Almería, 04120 Almería, Spain

[2] Department of Geology, FCFM, University of Chile, Santiago, Chile

[3] Andean Geothermal Center of Excellence (CEGA), Fondap-Conicyt, Santiago, Chile

areas of fruit and vegetable production in the whole of Europe, with a surface area under greenhouse cultivation exceeding 20,000 ha. The pronounced overexploitation of its groundwaters for irrigation and urban water supply has provoked a marked fall in piezometric levels, in addition to an advance in the saline front that has caused water salinization in some areas (Daniele et al. 2013a; Vallejos et al. 2015b). The structural complexity of this extensive aquifer system, combined with its lithological variability and the presence of numerous mineralizations dispersed across a fair proportion of its surface area (Daniele et al. 2013b), means that the physicochemistry of its groundwaters cover a wide range.

Various hydrochemical tools can be used to understand the processes that cause the chemical enrichment of the groundwaters (Sánchez et al. 2015). Hydrogeochemical and isotope analyses can additionally help to construct a conceptual model of the hydrogeological functioning of the aquifer with greater precision (Barbieri et al. 2005). Major, minor and trace ions can be very useful in identifying groundwater mixing or rock–water interactions, as well as in characterizing groundwater flows (Giménez-Forcada and Vega-Alegre 2015). The major ions allow differentiation of the most important causal processes of the bulk of the chemical load carried in the water, which arises from the interaction of the aqueous flow with the main lithological components of the aquifer medium. However, to understand the processes in more detail, it is necessary to turn to the minor ions. Thus, the concentration of ions like Ba or Sr will be controlled by the solubility of the barite and celestite, respectively (Hanor 2004; Underwood et al. 2009). Natural uranium present relates to the mobilization of this element from minerals and rocks that form the aquifer or adjacent geological formations (Liesch et al. 2015). For most of the minor elements (*i.e.* Li, F, Ti, V, Cr, Ni, Cu, Zn, As, Br, Rb, I and Cs), the high concentrations are related to high salinity waters, which are representative of the deep circulation inside the carbonate-evaporite aquifer (Morgantini et al. 2009). These aquifers are characterized by the presence of carbonate rocks (dolostone and limestone) with interlayers of more soluble mineral phases (*e.g.* anhydrite, gypsum and minor halite and fluorite) and are often confined under a low permeability cover (Chiodini et al. 1995). Groundwater circulation in the deep aquifer is generally characterized by long residence times. Radiogenic isotopes like ^{3}H or ^{14}C allow the mean residence times of the water in the aquifer to be determined (Xanke et al. 2015)—using tritium for periods of less than 60 years (Gonfiantini et al. 1998) and ^{14}C for older waters (Plummer 2005).

The purpose of this study was to determine the principal hydrogeochemical processes occurring in the Sierra de Gador aquifer, as well as the residence time of its waters. To this end, we analysed the ionic ratios of certain major, minor and trace ions and the values of stable and radioactive isotopes (July 2009). Additionally, the geochemistry of certain minor elements (*e.g.* barium, rubidium, uranium, caesium) supplies extra information on the coexistence of groundwater flows with different chemical compositions.

Hydrogeological setting

The study was carried out in the Sierra de Gador, situated in the province of Almeria in the extreme southeast of Spain (Fig. 1). The surface area of this coastal mountain chain is close to 1000 km^2. The climate is Mediterranean, characterized by warm, dry summers and mild winters. The amount of water available depends on the rainfall regime—and it rains seldom and irregularly. The semiarid character of the area arises due to the combination of a lack of precipitation (400 mm on the southern slopes of Sierra de Gador), strong insolation (around 2900 h $year^{-1}$), interannual variability in precipitation (22–35 %) and high potential evaporation (about 900 mm $year^{-1}$). Temperature increases from a mean of 16 °C on the top of the mountains to 18.7 °C at the foot. January is the coldest month (10 °C), and August is the hottest (27.2 °C) (Martín-Rosales et al. 2007). The inflows feeding the aquifers are basically infiltration from rainfall over the unit, as well as runoff from the slopes of the Sierra de Gador. Current outflows are almost exclusively the result of pumped abstractions.

Geologically, it belongs to the Internal Zones of the Betic Cordillera (Alpujarride Complex). The structure of the Alpujarride Complex is characterized by the superposition of a number of tectonic units or nappes. The entire superimposed nappe structure has been subject to important tensional and strike-slip events (Sanz de Galdeano et al. 1985), which have led to the development of basins, now filled with Neogene and Quaternary detrital material.

Two tectonic units have been identified in the area: Gador and Felix. The Gador unit consists of a basal layer of phyllite with quartzite intercalations, which has been assigned to the Permian–Triassic. The transition from this underlying formation to the limestone-dolomite layer above is usually a layer of calcoschist and marly limestone (Martin-Rojas et al. 2009). The upper part of the series is dolomitic, with limestone predominating towards the top. The whole series is approximately 1000 m thick. The formations of the Felix unit, like those of the Gador one, consist of a basal metapellitic layer with a carbonate layer above. The carbonate layer is much thinner than its Gador counterpart, normally less than 100 m. It is also Middle-Upper Triassic in age. The Gador unit covers almost all the

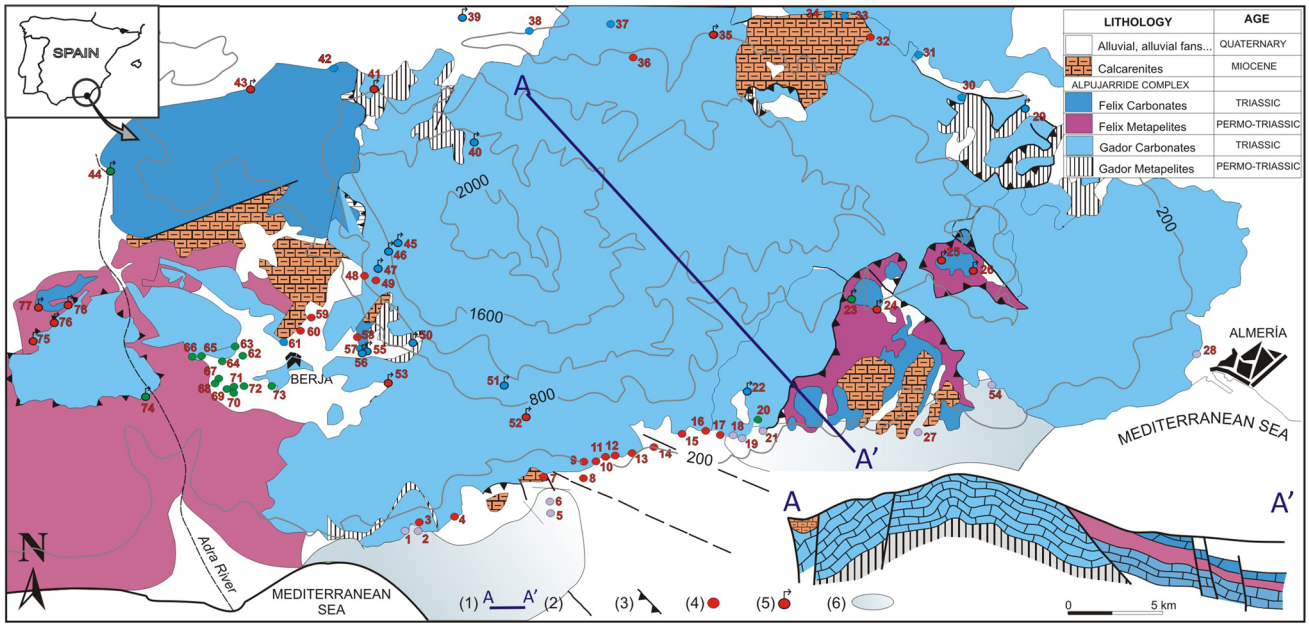

Fig. 1 Location of the study area and sampling points in different *colours* according to the groups identified. *1* cross section; *2* fault; *3* thrust fault; *4* well; *5* spring; *6* marine intrusion area

whole of Sierra de Gador, exposing small klippen of the overlying Felix unit.

Above these materials are the Miocene deposits, made up of calcarenite in the outcropping sectors, and marl and gypsum beneath a Plioquaternary infill (Rodríguez-Fernández and Martín-Penela 1993). Quaternary deposits are present along the whole of the base of the southern face of the Sierra, making up large alluvial fans that occasionally exceed 150 m in thickness. In the western sector, the Berja intra-mountain basin is filled with Neogene and Quaternary deposits. The carbonates of the Gador and Felix units are highly permeable. The schist, phyllite and quartzite of both Alpujarride units are practically impermeable. With respect to the post-orogenic materials, the Miocene and Pliocene calcarenite and the Quaternary materials are also permeable. The Sierra de Gador aquifers are geometrically complex as a consequence of the intense alpine compressional tectonics of the region.

Numerous reconnaissance boreholes have provided evidence of their structural complexity by revealing the variable thicknesses of Quaternary materials and the faulting, which has resulted in substantial vertical and horizontal compartmentalization of the carbonate rocks.

Materials and methods

A sampling survey was carried out to monitor water quality and assess the main physicochemical processes in this aquifer. In July 2009, 78 samples of groundwater were collected from springs and wells (Fig. 1). The springs of Sierra de Gador show high discharge variability (70 % of the springs less than 5 L/s and the rest 20–100 L/s). The wells have a varying depth, between a few and a hundred of metres. Temperature, electrical conductivity (EC) and pH were determined in situ. Alkalinity (as HCO_3) was determined by titration at the time of sampling. Samples were taken in duplicate, filtered using a 0.45-μm Millipore filter and stored in polyethylene bottles at 4 °C. For cation analysis, one bottle of each sample was acidified to pH < 2 with environmental grade (ultra-pure) nitric acid to avoid problems of absorption or precipitation (Vallejos et al. 2015b). Sample composition was determined by means of an ICP-Mass Spectrometer at Acme Labs (Vancouver, Canada). The analytical results obtained are summarized in Table 1.

The mineral saturation indices (SI) indicate the degree of saturation in a particular mineral phase compared to the aqueous solution in contact. Based on this SI value, the trend of precipitation or dilution of the mineral phases can be deduced. The SI was obtained using the PHREEQC code, version 3 (Parkhurst and Appelo 2013). According to the characteristics of the study plot, the phases analysed were calcite, dolomite, gypsum and halite (Vallejos et al. 2015b).

$\delta^{34}S_{SO4}$, $\delta^{18}O_{SO4}$ and $\delta^{18}O_{H2O}$ isotope measurements were determined at the Stable Isotope Laboratory of the Zaidin Experimental Station (Granada, Spain). The pretreatment of samples for isotope analysis $\delta^{34}S$ and $\delta^{18}O$ from SO_4 implies to convert the sulphate to $BaSO_4$ by the addition of barium chloride. Firstly, it was necessary to acidify the samples with HCl, to get the pH below 3.5. In

Table 1 Results of chemical analyses of water samples

Sample	Group	Class	T (°C)	EC μS/cm	pH	Cl mg/L	SO_4	HCO_3	Na	Mg	Ca	K	Br
1	G4	A	26	1549	7.44	405.6	64.2	250.1	138.1	66.0	79.8	3.6	0.10
2	G4	A	25.4	1115	7.55	240.3	61.5	256.2	83.2	52.2	67.5	2.9	0.06
3	G2-B	A	25.3	782	7.88	71.1	76.1	292.8	40.9	39.5	63.7	2.7	0.04
4	G2-B	A	24.1	827	7.53	123.2	59.1	286.7	49.4	44.2	63.1	3.0	0.05
5	G4	A	27.4	1080	7.71	228.3	53.5	286.7	101.4	42.9	55.4	5.6	0.06
6	G4	A	24.2	1040	7.85	183.3	41.3	250.1	53.3	49.5	75.6	2.0	0.05
7	G2-B	B	22.8	557	7.7	31.0	42.7	280.6	17.6	32.7	54.2	1.2	0.03
8	G2-B	A	24.2	670	7.54	96.1	38.7	256.2	34.1	38.0	51.2	2.7	0.03
9	G2	B	21.8	403	7.66	27.0	20.1	207.4	12.8	25.2	38.8	1.0	0.02
10	G2	B	21.6	460	7.72	43.1	19.0	219.6	21.0	26.5	41.6	1.0	0.02
11	G2-B	B	21.5	419	7.63	27.0	20.9	219.6	13.6	26.5	41.4	1.0	0.08
12	G2-B	B	20.9	459	7.6	32.0	18.2	237.9	15.4	28.4	45.9	0.9	0.03
13	G2-B	B	20.5	453	7.56	28.0	25.2	244.0	13.8	29.3	44.8	0.9	0.03
14	G2-B	A	26.1	502	7.44	21.0	35.0	280.6	12.1	35.1	50.3	1.9	0.02
15	G2-B	B	22.8	548	7.62	33.0	33.8	298.9	16.3	30.0	54.4	5.3	0.02
16	G2	A	22.7	570	7.46	26.0	50.9	298.9	13.8	38.6	57.9	1.8	0.03
17	G2	A	23.3	664	7.64	60.1	40.5	280.6	27.6	35.6	53.1	6.6	0.02
18	G4	B	21.5	1046	7.91	229.3	40.2	256.2	71.1	41.0	80.0	1.3	0.02
19	G4	A	20.7	1579	7.58	329.5	57.7	256.2	140.0	47.8	105.3	6.0	0.05
20	G3	B	22.5	1072	7.35	211.3	50.6	305.0	66.5	46.8	86.3	1.3	0.30
21	G4	A	15.9	3380	7.49	784.1	98.7	213.5	396.6	78.8	148.4	3.1	0.56
22	G1	B	16.8	541	7.42	26.0	8.8	347.6	10.4	27.9	69.9	0.7	0.13
23	G3	B	17.3	326	8.17	11.0	6.0	195.2	6.8	25.5	31.4	0.3	0.33
24	G2	B	18.9	449	7.7	22.0	36.2	250.1	11.9	25.6	48.3	5.1	0.11
25	G2	B	16.3	390	7.76	12.0	7.8	262.3	6.8	29.5	40.2	0.5	0.18
26	G2	B	17.4	394	7.8	17.0	19.6	268.4	8.3	30.5	36.0	0.5	0.11
27	G4	A	22.6	2930	7.55	761.1	292.3	317.1	371.3	95.5	114.4	6.9	0.12
28	G4	A	27.8	1266	7.55	256.4	89.5	317.1	152.6	45.7	44.9	9.3	0.09
29	G1	A	42.5	915	7.03	19.0	217.3	384.2	19.4	42.6	123.5	4.2	0.07
30	G1	A	30.9	932	7.36	15.0	224.7	445.2	8.9	47.7	127.4	9.5	0.11
31	G1	A	28.9	839	7.19	15.0	140.6	445.2	10.7	49.3	105.3	6.9	0.08
32	G2	A	22.7	939	6.98	25.0	92.7	616.0	9.4	70.3	124.7	4.6	0.22
33	G1	A	22.7	980	7.08	16.0	120.6	561.1	8.3	62.2	129.6	1.2	0.08
34	G1	A	24.1	967	7.01	12.0	182.1	512.3	7.4	59.8	122.7	3.1	0.06
35	G2-B	B	18.2	561	7.55	10.0	34.9	378.1	4.9	35.0	63.2	3.6	0.08
36	G2-B	A	20.1	599	7.68	10.0	54.3	365.9	6.8	39.3	70.6	1.0	0.07
37	G1	B	16.7	538	8.44	9.0	79.7	283.6	6.2	30.0	77.5	0.9	0.05
38	G1	A	19.1	765	7.85	17.0	170.9	347.6	15.3	36.0	115.0	1.0	0.06
39	G1	B	15.2	368	7.58	6.0	61.6	189.1	3.7	16.4	54.7	2.5	0.03
40	G1	B	12.1	259	8.18	4.0	3.5	219.6	1.4	17.9	30.9	0.3	0.09
41	G2	B	14.4	271	7.97	7.0	13.4	161.7	3.2	17.9	30.9	0.5	0.04
42	G1	A	23.2	859	7.16	17.0	179.9	414.7	17.9	52.3	113.2	2.7	0.17
43	G2	A	20.6	676	7.95	24.0	112.7	305.0	23.3	38.6	75.2	1.6	0.04
44	G3	A	24.1	740	8.71	45.1	152.4	247.0	41.3	38.0	72.7	3.2	0.02
45	G1	B	8.9	301	8.07	3.0	17.6	189.1	1.4	14.9	38.7	2.5	0.08
46	G1	B	17.1	345	8.42	5.0	65.5	164.7	3.7	19.7	38.0	0.5	0.07
47	G2	B	17.8	356	8.12	9.0	42.3	207.4	7.4	23.5	42.0	0.5	0.23

Table 1 continued

Sample	Group	Class	T (°C)	EC µS/cm	pH	Cl mg/L	SO_4	HCO_3	Na	Mg	Ca	K	Br
48	G2	A	23.4	844	7.41	43.1	122.3	372.0	29.1	53.6	72.5	3.9	0.07
49	G2	B	23.7	384	8.43	8.0	33.3	201.3	7.4	22.6	41.3	0.3	0.04
50	G1	B	16.7	483	8.09	7.0	108.3	201.3	2.7	27.1	58.5	3.6	0.06
51	G1	B	16.7	302	7.93	5.0	10.7	213.5	2.0	20.0	35.9	0.4	0.07
52	G2	B	15.2	300	8.13	5.0	13.1	231.8	1.8	20.4	35.3	0.5	0.72
53	G2	B	20.6	536	7.75	14.0	82.3	244.0	11.4	30.2	55.2	1.4	0.05
54	G4	A	24.1	1735	7.4	347.5	72.4	286.7	142.9	60.0	114.2	2.2	0.10
55	G1	B	18.5	553	7.71	6.0	132.1	207.4	4.2	26.0	61.1	2.2	0.10
56	G1	B	18	557	7.87	8.0	141.3	207.4	3.5	30.1	71.6	4.7	0.26
57	G1	B	17.1	542	7.85	10.0	135.6	201.3	3.7	33.2	70.7	0.8	0.31
58	G2	B	17.9	611	7.69	15.0	125.8	237.9	14.2	34.0	67.1	0.9	0.31
59	G2	A	21.1	1072	7.47	52.1	127.4	396.4	40.4	74.7	76.2	3.1	0.29
60	G4	B	20.3	761	7.47	16.0	168.2	359.8	11.5	42.9	91.0	5.1	0.23
61	G1	B	20.3	734	7.52	14.0	172.8	280.6	9.4	41.3	88.7	5.4	0.23
62	G3	B	20.3	1479	7.26	42.1	456.9	115.9	22.9	125.1	139.4	16.0	0.61
63	G3	A	24.2	1428	7.46	126.2	321.1	341.5	62.2	84.6	123.5	3.4	0.36
64	G3	A	22.4	1464	7.48	153.2	183.1	291.5	22.0	62.0	86.7	55.2	0.57
65	G3	A	22.7	1228	7.34	109.2	218.0	323.2	67.7	67.1	96.6	4.2	0.13
66	G3	A	21.9	1155	7.45	106.1	214.3	268.4	64.9	56.5	98.5	5.2	0.07
67	G3	B	20.1	1556	7.27	65.1	515.1	372.0	32.4	116.0	161.8	6.9	0.67
68	G3	B	21.5	1478	7.3	47.1	364.5	402.5	33.4	107.6	158.4	3.8	1.46
69	G3	B	19.2	2260	7.18	121.2	664.1	463.5	48.4	191.0	216.3	7.9	0.86
70	G3	B	20.4	1782	7.17	68.1	490.8	463.5	43.5	135.5	183.3	6.6	0.80
71	G3	B	19.7	1853	7.23	70.1	464.6	475.7	45.3	144.7	183.2	5.3	0.69
72	G3	B	20.2	1701	7.1	75.1	509.1	445.2	39.4	128.7	183.0	3.4	0.80
73	G3	B	20.3	974	7.5	30.0	213.4	320.2	26.9	61.7	105.7	5.8	1.18
74	G3	A	24.4	2530	8.01	369.5	565.6	341.5	230.0	80.9	252.7	8.2	3.18
75	G2	B	16.5	415	6.62	16.0	20.9	237.9	10.7	26.8	31.3	4.2	2.75
76	G2	B	18.3	329	8.05	11.0	13.0	201.3	4.5	19.5	31.1	4.2	0.67
77	G2	B	17.9	343	8.3	13.0	21.6	195.2	5.9	26.2	21.4	5.0	1.27
78	G2	B	20.3	331	9.12	16.0	16.0	201.3	6.4	20.4	27.8	7.1	0.07
SW			15.3	55.000	8.32	21,308.0	3426.0	35.4	13,584.0	1564.0	468.0	412.0	73.0

Sample	Ba	Cs	Li	Rb	Si	Sr	U	Saturation index		
	µg/L							Barite	Celestite	Gypsum
1	202	1.0	9.2	2.6	5651	1763	3.2	0.29	−1.86	−1.93
2	153	0.7	8.9	2.0	5604	1392	3.3	0.23	−1.93	−1.95
3	85	0.5	8.4	1.9	5920	1258	3.9	0.11	−1.83	−1.84
4	135	0.8	7.0	1.8	5903	1230	3.6	0.22	−1.96	−1.96
5	124	1.7	18.2	3.8	7546	1897	1.4	0.12	−1.83	−2.08
6	265	0.5	4.8	1.6	6050	874	2.0	0.33	−2.27	−2.06
7	112	0.3	2.7	0.7	5265	542	2.8	0.09	−2.39	−2.1
8	107	1.0	8.1	2.1	6128	855	2.0	−0.02	−2.25	−2.19
9	196	0.2	1.7	0.5	4486	264	1.4	0.09	−2.97	−2.5
10	202	0.2	4.7	0.5	4359	277	1.5	0.07	−2.98	−2.51
11	185	0.2	1.9	0.5	4581	285	1.4	0.09	−2.93	−2.47
12	193	0.3	1.9	0.5	4672	255	1.8	−0.03	−3.05	−2.5

Table 1 continued

Sample	Ba	Cs	Li	Rb	Si	Sr	U	Saturation index		
	µg/L							Barite	Celestite	Gypsum
13	170	0.2	4.0	0.5	4592	249	1.6	0.13	−2.92	−2.37
14	124	0.5	5.1	1.6	5999	657	1.2	0	−2.39	−2.22
15	150	0.3	2.6	0.8	5100	280	2.4	0.13	−2.77	−2.19
16	88	0.4	4.5	1.4	5674	504	1.5	0.05	−2.37	−2.01
17	61	0.1	4.9	2.2	5464	425	2.1	−0.22	−2.53	−2.14
18	220	0.4	3.0	0.9	4540	495	2.4	0.3	−2.54	−2.04
19	183	0.5	3.7	1.2	4421	548	2.9	0.32	−2.4	−1.82
20	231	0.3	3.8	0.8	5111	530	2.8	0.38	−2.43	−1.93
21	262	0.4	3.8	1.2	3359	466	1.5	0.65	−2.38	−1.57
22	21	0.0	1.4	0.3	3527	173	0.7	−0.76	−2.81	−2.2
23	9	0.0	0.7	0.1	3761	38	0.1	−1.64	−4.28	−3..09
24	45	0.0	0.8	0.8	2933	87	0.3	−0.27	−3.22	−2..18
25	28	0.0	0.7	0.1	3294	46	0.3	−1.05	−4.14	−2.9
26	34	0.0	1.6	0.1	3923	79	0.6	−0.6	−3.52	−2.55
27	80	0.5	11.9	4.0	6321	944	4.9	0.41	−1.64	−1.26
28	80	1.0	25.8	5.3	6136	687	3.8	0.06	−2.08	−1.97
29	61	18.9	63.1	13.6	13.740	2548	2.3	0.03	−1.16	−1.21
30	37	9.2	23.2	7.5	8572	2700	1.6	−0.02	−1.14	−1.19
31	53	6.0	25.4	6.3	7557	1896	2.6	0.01	−1.44	−1.43
32	85	1.4	13.6	2.1	5916	1194	4.4	0.12	−1.89	−1.58
33	52	1.6	10.8	2.1	6027	1447	3.6	0.02	−1.69	−1.44
34	41	2.0	11.5	2.8	5736	1697	2.3	0.04	−1.44	−1.29
35	94	0.3	2.4	0.9	4279	223	2.5	0	−2.88	−2.13
36	65	0.6	4.5	1.1	4234	338	2.8	−0.03	−2.53	−1.92
37	40	0.1	4.2	0.5	4050	744	1.6	−0.02	−2.01	−1.69
38	59	0.0	6.4	0.5	10.076	902	2.5	0.33	−1.68	−1.28
39	65	0.0	3.1	0.5	4395	785	1.1	0.17	−2	−1.86
40	14	0.0	0.3	0.1	1586	61	0.2	−1.58	−4.3	−3.29
41	48	0.0	1.1	0.1	3401	227	0.5	−0.49	−3.15	−2.71
42	38	2.1	26.8	3.5	5797	1831	3.4	0.07	−1.4	−1.31
43	39	0.1	20.0	0.7	5445	936	2.5	0.01	−1.8	−1.6
44	36	0.3	89.6	1.9	6146	1064	3.2	0	−1.62	−1.51
45	26	0.0	4.6	0.4	3191	198	0.4	−0.54	−3.07	−2.48
46	45	0.0	1.0	0.2	3673	508	0.5	0.03	−2.16	−1.99
47	47	0.0	1.8	0.3	3808	571	0.9	−0.15	−2.31	−2.15
48	37	0.9	18.6	4.3	5461	1817	3.9	−0.07	−1.51	−1.62
49	48	0.0	1.5	0.2	3892	400	0.7	−0.33	−2.56	−2.27
50	34	0.0	1.5	0.4	3530	915	2.8	0.06	−1.76	−1.65
51	111	0.0	0.7	0.2	3452	303	1.5	−0.29	−3.14	−2.77
52	188	0.0	0.8	0.3	3508	481	1.4	0.06	−2.85	−2.69
53	45	0.1	2.8	0.4	4668	770	2.2	0	−1.95	−1.8
54	87	0.4	5.5	1.3	5026	863	2.8	0	−2.14	−1.73
55	34	0.0	2.1	0.4	3459	1440	2.5	0.04	−1.5	−1.56
56	38	0.2	2.8	0.6	4059	1566	2.8	0.15	−1.44	−1.48
57	36	0.0	2.7	0.4	4149	1653	3.0	0.12	−1.44	−1.51
58	52	0.1	3.5	0.5	4495	1348	2.6	0.25	−1.69	−1.56
59	104	0.4	10.8	1.7	6931	1062	4.3	0.38	−1.77	−1.62

Table 1 continued

Sample	Ba	Cs	Li	Rb	Si	Sr	U	Saturation index		
	µg/L							Barite	Celestite	Gypsum
60	58	0.1	4.1	1.0	4604	2077	3.7	0.31	−1.32	−1.38
61	57	0.1	4.0	1.2	4840	1975	3.6	0.26	−1.32	−1.37
62	68	0.2	9.4	2.4	6296	3382	7.0	0.57	−0.85	−0.94
63	45	15.1	148.9	10.6	6450	3295	6.7	0.24	−1.11	−1.11
64	50	17.2	105.3	12.2	6022	3084	8.8	0.19	−1.16	−1.42
65	53	18.6	94.3	11.7	6356	3295	8.4	0.25	−1.07	−1.31
66	64	18.3	101.0	12.2	6142	3507	7.9	0.33	−1.04	−1..3
67	71	0.0	9.1	1.5	7059	3810	7.0	0.62	−0.77	−0.85
68	49	0.1	12.0	0.6	7172	2878	7.0	0.32	−1.03	−0.99
69	67	0.0	19.3	0.6	9378	5075	10.9	0.63	−0.65	−0.72
70	50	0.1	13.3	0.5	7780	3164	8.2	0.42	−0.91	−0.85
71	63	0.0	15.2	0.7	8508	3616	9.1	0.51	−0.88	−0.87
72	42	3.0	15.3	4.9	10.561	4581	9.5	0.34	−0.72	−0.83
73	65	0.0	7.1	1.0	5655	2164	4.9	0.36	−1.24	−1.26
74	36	64.5	553.8	42.0	6232	5708	6.3	0.23	−0.63	−0.69
75	25	0.0	3.2	0.4	4025	146	2.3	−0.67	−3.18	−2.56
76	28	0.0	1.3	0.2	4118	112	0.4	−0.79	−3.49	−2.74
77	30	0.0	1.7	0.4	3935	102	0.8	−0.58	−3.32	−2.7
78	19	0.0	1.3	0.3	4060	234	0.6	−0.97	−3.09	−2.75
SW	19	0.0	0.2	131	500	8.45	3.2			

EC electrical conductivity. Location of sampling points in Fig. 1

this way, the co-precipitation of others barium salts is avoided. $\delta^{18}O_{H2O}$ determination was carried out using a Gas Bench II Analyses (GC-IRMS), $\delta^{34}S_{SO4}$ with a Fisons NA 1500 NC elemental analyser and $\delta^{18}O_{SO4}$ using a thermal conversion elemental analyser (Thermo Finnigan TC/EA). The analytical uncertainties (1σ) for $\delta^{34}S$, $\delta^{18}O_{SO4}$ and $\delta^{18}O_{H2O}$ are ±0.1, ±0.5 and ±0.2 ‰, respectively.

Forty-three groundwater samples were collected for ^{3}H analysis in 1 L high-density polyethylene bottles. The samples were analysed at the University of Miami Tritium Laboratory (USA). Tritium was measured by internal Gas Proportional Counting of H^2 gas made from the water sample. Low-level water samples go through an electrolytic enrichment step whereby tritium concentrations are increased about 60-fold by means of volume reduction. Accuracy of the low-level measurement with enrichment is 0.10 TU (0.3 pCi L^{-1} of H_2O, Vallejos et al. 2015b).

In addition, eight measurements of ^{14}C activity with $\delta^{13}C$ were available. These samples were analysed at Hertelendi Laboratory of Environmental Studies (Debrecen, Hungary). The ^{14}C activities were measured by precipitation of TDIC in the form of $BaCO_3$. The volume of the sampling container is usually 60 l, which is sufficient for extracting about 2.5 g of carbon from water with a concentration of about 250 ppm of bicarbonates. $BaCl_2$ solution is added to the water sample after adjusting the pH to convert all bicarbonates to carbonates (carbon-free concentrated NaOH is added until pH reaches about 8.5). Normally such a precipitate is fine grained and requires a day to settle completely. Carbon dioxide is evolved from the precipitate by adding concentrated H_2SO_4 or H_3PO_4. The chemically pretreated sample is combusted or acid digested CO_2 being obtained in a controlled oxygen stream. Gaseous impurities are removed by passing the produced CO_2 through a hot copper furnace. The purified CO_2 is trapped into stainless steel vessel and measured by gas proportional counting. The precision was ±0.5 ‰ pMC for ^{14}C activities.

Results and discussion

Major constituents

The chemical composition of groundwater samples along Sierra de Gador shows the complexity of this aquifer system is mainly determined by its lithology. In order to characterize the hydrochemistry of the groundwater based on major ions, the analytical data were plotted on a modified Durov diagram (Fig. 2). In this diagram, the cation and anion triangles are recognized and separated along the

25 % axes so that the main field is conveniently divided into nine subfields (Al-Bassam et al. 1997; Al-Bassam and Khalil 2012). Four groups can be recognized according to the data distribution on this graph. These groups were identified as G-1, G-2, G-3 and G-4. Group G-1 is characterized by calcium bicarbonate samples with low mineralization. G-2 contains samples that are more magnesic than G-1, apparently affected by a process of dolomite dissolution. The calcium–magnesium–bicarbonate facies from groups (G-1 and G-2) indicates recharge from limestone and dolostone, main rock of this aquifer system. Group 3 shows the influence of sulphate dissolution, and samples have a higher saline content than in G-1 or G-2. G-4 contains the samples with the highest saline content, some of which have a sodium chloride facies. This fact, and their proximity to the coast, could indicate that these samples are affected by marine intrusion.

The relationships among some major ions were studied with the goal of recognizing the main hydrogeochemical processes that affect the defined groups. Figure 3a shows the relationship for HCO_3 versus $Ca + Mg\text{-}SO_4$. This relationship reveals the carbonate dissolution processes excluding the influence of sulphate. The 1:1 line depicts the dolomite dissolution processes. Samples from G-1 and G-2 are distributed along this straight line, while those from G-3 and G-4 are above the line. In order to determine the sulphate influence, the $HCO_3 + SO_4$ versus $Ca + Mg$ graph was used (Fig. 3b). In this case, samples from G-1, G-2 and G-3 are on the 1:1 line showing that the carbonate and sulphate dissolution are the dominant processes affecting these samples. The sulphate influence on samples in G-3 is remarkable. On the other side, samples in G-4 show an excess in Ca or Mg linked to an additional contribution of Mg due to marine processes. The marine influence on G-4 samples can be determined thanks to the graph Cl vs. Br (Fig. 3c), being the distribution of G-4 samples close to the line defined by Cl/Br seawater ratio (Vengosh et al. 1999).

Figure 3d, which shows the relationship between Mg and HCO_3, clarifies which processes determine the ion distribution of the samples. A ratio of 1:2 indicates congruent dissolution of dolomite. Groups G-1 and G-2 are slightly about this ratio. Nevertheless, samples in group G-3 clearly have an excess of magnesium. The process that could explain this is dedolomitization. An excess of dissolved calcium is produced as a consequence of the

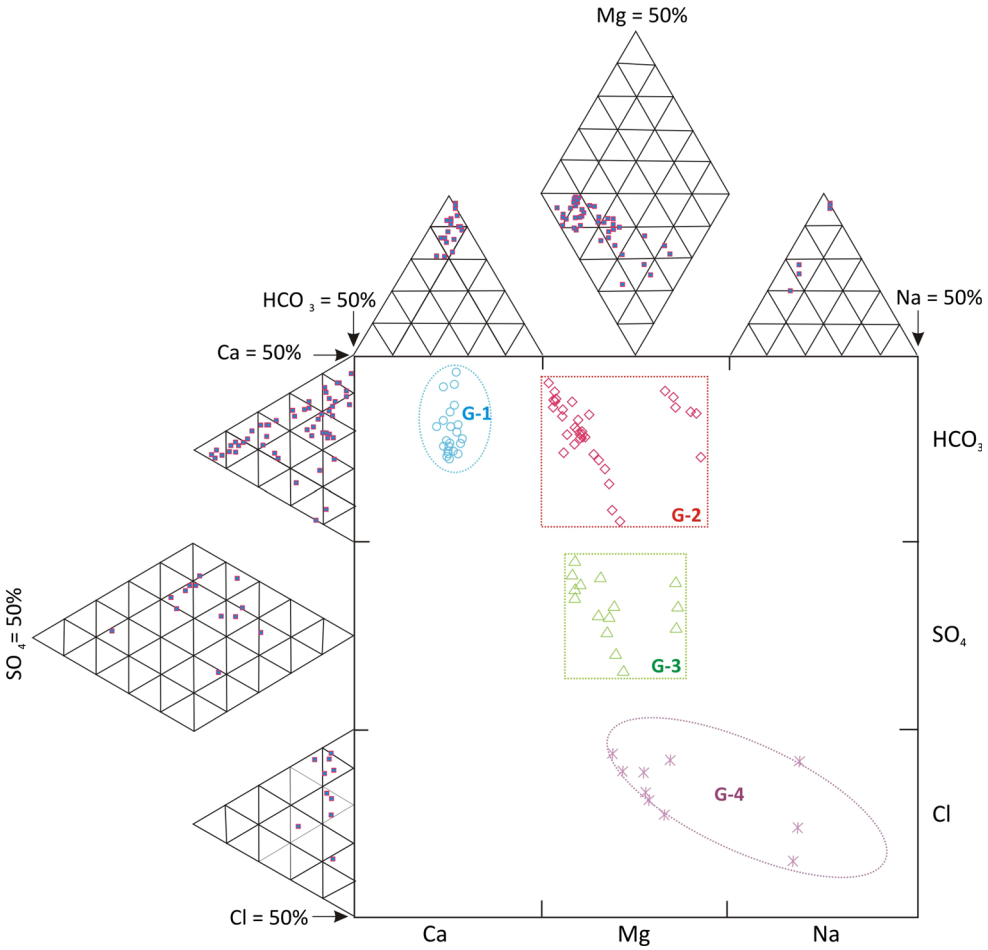

Fig. 2 Expanded Durov diagram corresponding to groundwater samples

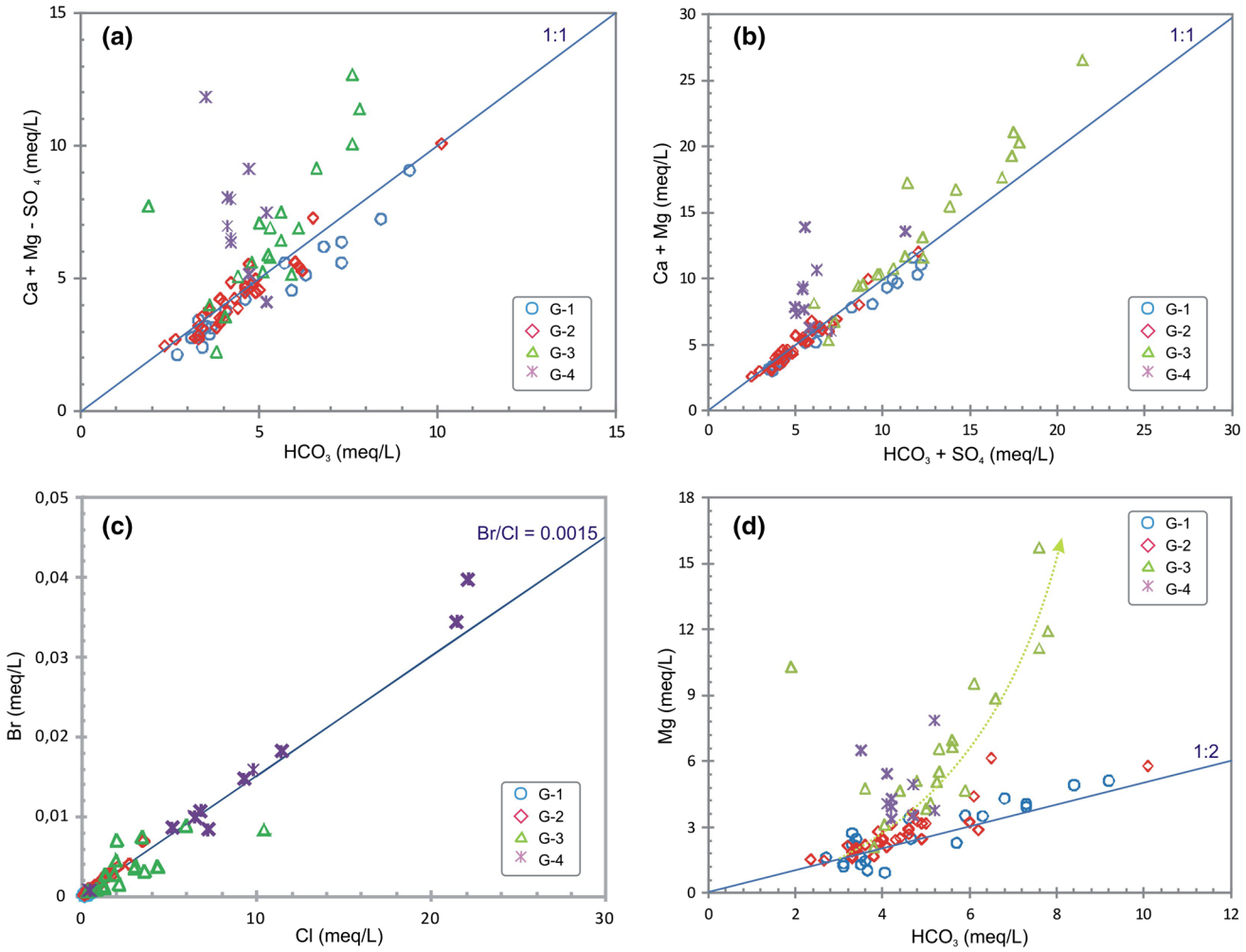

Fig. 3 Hydrochemical relationships between selected major ions in groundwater. The freshwater–seawater mixing line has been included (3c)

dissolution of gypsum; it provokes the precipitation of calcite, so increasing the quantity of dissolved magnesium (Back et al. 1983; Deike 1990; Saunders and Toran 1994; Ma et al. 2011). The net result is that the dissolution of gypsum induces the transformation of dolomite to calcite in the rock and produces waters with increased Mg^{2+}. Approximately 95 % of the SI values for calcite and dolomite in the groundwater samples were greater than zero (Vallejos et al. 2015b).

Minor and trace elements

The analysis of minor and trace elements can assist in recognizing hydrogeochemical processes that are not always detected using the major ions. Here, we studied the ion ratios of the minor ions Ba and Sr with sulphate. Figure 4a shows two clearly differentiated trends in the distribution of samples pertaining to the SO_4^{2-}/Ba^{2+} ratio. Samples in groups 1 and 3 reflect a relatively constant concentration in barium, independent of its sulphate content. The samples in group 2 do not respond in the same way; rather, some of them are distributed in a similar way to groups 1 and 3, while the rest show an increase in concentration in barium and a low sulphate content. These samples were reclassified as group 2b. The samples in group 4 behave in a similar way to these. The high values of Ba detected in these samples do not have any relationship with marine intrusion because the barium concentration in seawater is around 20 µg/L, lower than the Ba measured in samples from G-4.

With respect to the SO_4^{2-}/Sr^{2+} ratio (Fig. 4b), one can see how the samples are clearly aligned, except for samples from 2b and 4, where the variations in strontium concentration are not accompanied by changes in sulphate concentration. The linear relationship is a consequence of the gypsum dissolution. The strontium is part of gypsum structure (Hanor 2004; Stamatakis et al. 2009). This relationship is not evident in samples from groups 2b and 4. These samples come from along the southern face of the Sierra de Gador (Fig. 1), where there are very few

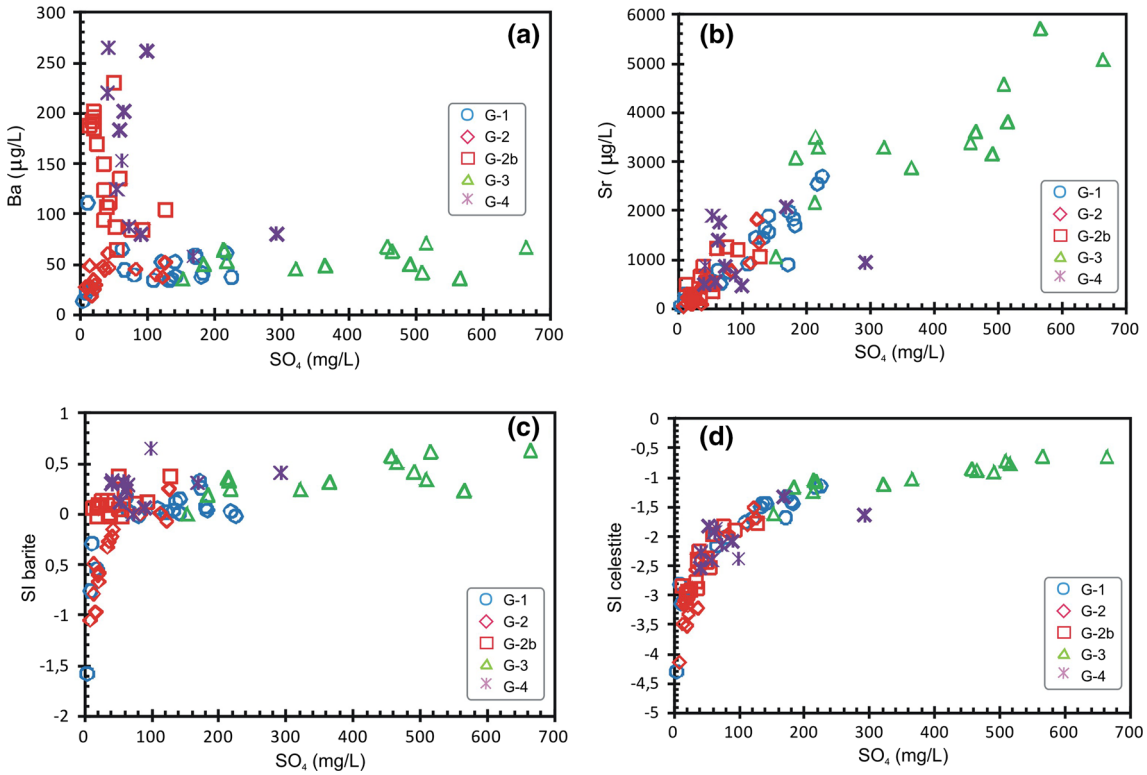

Fig. 4 Barium, strontium, saturation index of barite and saturation index of celestite versus sulphate concentration (mg/L) of groundwater

intercalated gypsums within the limestone, hence the low sulphate concentrations in the samples. The increment in strontium would be linked to a longer residence time of this water, which increases the concentration of this ion in dissolution. Something similar occurs with barium. The increment in barium observed in these samples is not related to their sulphate concentration. The samples belonging to these groups were taken from deep boreholes where the flow was probably part of a slow, regional flow; this would favour concentration in these ions. In turn, samples in groups 1, 2 and 3 had higher sulphate and lower barium concentrations. These low concentrations of barium would be a result of barite precipitation. An increase in sulphate favours saturation in barite and its precipitation, so that the concentration of dissolved barium is reduced (Underwood et al. 2009; Giménez-Forcada and Vega-Alegre 2015).

The saturation index for barite and celestite was calculated for all samples (Fig. 4c, d). The saturation index for celestite shows an exponential increase as a function of the sulphate content; no positive value was obtained in any sample, and so its precipitation can be disregarded. 80 % of the samples had positive saturation indices for barite. The exponential trend is similar to that obtained for celestite, though the fit is not as precise. Samples in groups 2b and 4 presented SI between 0 and 0.2 and a heterogeneous distribution in terms of the defined trend-line. This might indicate that the waters sampled are close to saturation due to their high barium concentrations but that they have not precipitated because of their low sulphate content.

To explain the trends in SO_4^{2-}/Ba^{2+} ratio observed in the samples from groups 2b and 3, a hydrogeochemical modelling was carried out whereby, starting from a sample rich in Ba and poor in SO_4 (type group 2b), we can obtain a water poor in Ba and rich in SO_4 (type group 3) by adding gypsum to the dissolution process in a ten stages. The quantity of gypsum added was 6.12 mmol, in accordance with the compositional difference between the end members. As shown in Fig. 5, the addition of the sulphate ion produces a gradual increase in the saturation indices of barite and gypsum. In the case of barite, it goes from values of the SI close to zero (corresponding to measurements from samples in group 2b) to values of around 1 (*i.e.* slightly higher than those observations for group 3). In the case of gypsum, the evolution of the simulated saturation indices fits the measured ones. The low barium concentrations observed in group 3 samples are a consequence of the increase in the SI of barite due to the dissolution of sulphate. This reduction in barium, consequence of the precipitation in barite, explains the observations shown in Fig. 4.

The analyses corresponding to trace elements can help us to interpret additional processes that are taking place in the aquifer system. Some ion ratios allow differentiation between the two classes of samples, A and B, according to

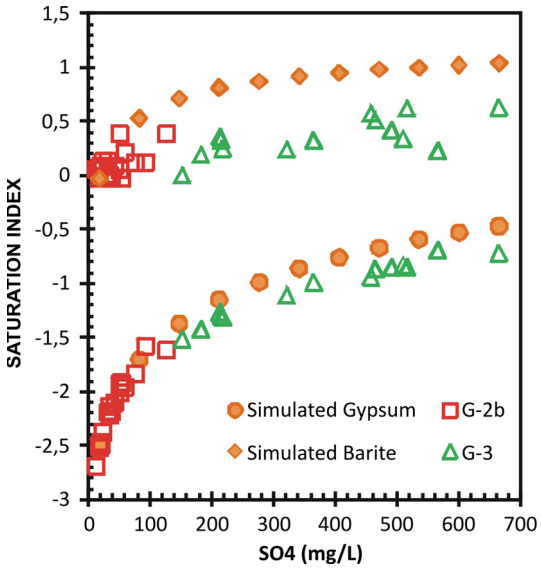

Fig. 5 Comparison between barite and gypsum saturation indices obtained with measured and simulated water versus sulphate concentration (mg/L). The simulated data were obtained from an initial sample, adding gypsum in ten steps

two well defined trends (Fig. 6). These trends can be observed in the Rb/Sr ratio (Fig. 6a), where Rb concentration increases according to an exponential distribution function with respect to Sr (class A) and, in contrast, where the Rb values remain constant and independent of the Sr concentration (class B). In terms of the U/Li ratio, samples in class B were positively aligned in accordance with the increase in both uranium and lithium concentrations. Nevertheless, the samples classified as A do not exhibit any relationship existing between these two ions (Fig. 6b). These different patterns of enrichment in trace ions in the two classes could be linked to contrasting flow patterns. The samples belonging to class A—which show higher rates of ionic enrichment in trace elements than in class B—could be determined by slower and/or deeper flowpaths that are more regional in nature, *i.e.* covering greater distances. In general, these samples had higher temperatures than the corresponding samples from class B (Table 1).

The concentrations in uranium in the analysed samples showed a highly significant correlation with silica for class B (Fig. 6c). This would be an indicator that the bulk of the uranium has a detritic source. In fact, the samples with the highest uranium concentrations (>7 μg/L) were taken from boreholes in the Berja basin (Fig. 1), where detritic sediments overlie the Triassic carbonates. The samples in class A do not show this correlation, probably as a consequence of the thermal character of these waters, which favours the mobilization of these ions (Valentino and Stanzione 2003). The effect of temperature in the class A samples is particularly obvious for ions like Rb and Cs, causing them to be mobilized and incorporated into the groundwater. Figure 6d shows how the increase in such ions in samples of class A is linear above a concentration of 5 μg/L in Rb, while it is practically nil for the remainder of the samples in this class and in class B.

The differentiation of samples into two classes, A and B, established from the ion ratios between certain minor and trace ions was utilized to see whether the behaviour in groups 1, 2, 3 and 4, established from the ion ratios of the major ions, is homogeneous. The criterion to distinguish the classes A and B has been only geochemical. Nevertheless, there is a clear correlation between class A and deep samples and class B and shallow samples, due to the fact these classes are differentiated by their regional character and residence time. Classes A and B are conditioned by temperature and by the velocity and length of the flowpath. With the aim of discovering whether these factors condition the major ion content of the groundwaters, we plotted graphs of SO_4 vs. Ca and HCO_3 vs. Mg, which identify the various groups subdivided according to whether they belong to class A or B (Fig. 7). Group 4 is not included in either graph given that external processes (marine intrusion) affect the ionic content of certain ions like Mg, as well as temperature, so masking any other processes occurring. Figure 7a shows that the established groups can be differentiated by looking at the class to which they belong. The differentiation between classes A and B is clear for the samples belonging to group 1, and this is also true for samples in group 2. In both groups, samples in class A exhibit higher ion concentrations than samples in class B; this is explained by a more effective dissolution as a consequence of the more regional character of the flows and the higher temperatures. Samples in group 3 also show a different distribution between A and B. However, in this case, the ion concentrations of the samples belonging to class B are higher than in class A. Samples belonging to 3-B were taken from boreholes in a part of the carbonate aquifer overlain by detritic deposits, with abundant intercalated layers of gypsum. The results obtained based on the HCO_3/Mg ratio (Fig. 7b) are very similar. There is a good differentiation between groups 1 and 2 belonging to classes A and B, though this is not true for the samples in group 3. In this case, the 3-B samples have higher sulphate concentrations, since they are affected more by a dedolomitization process, which in the end leads to a greater enrichment in bicarbonate and magnesium.

Isotopic composition of groundwater

Sulphur isotopes of sulphate ($\delta^{34}S$ and $\delta^{18}O$)

The use of several isotopes, coupled with hydrogeological and hydrochemical information, has proved to be a useful tool for assessing the origin of solutes. Krouse (1980)

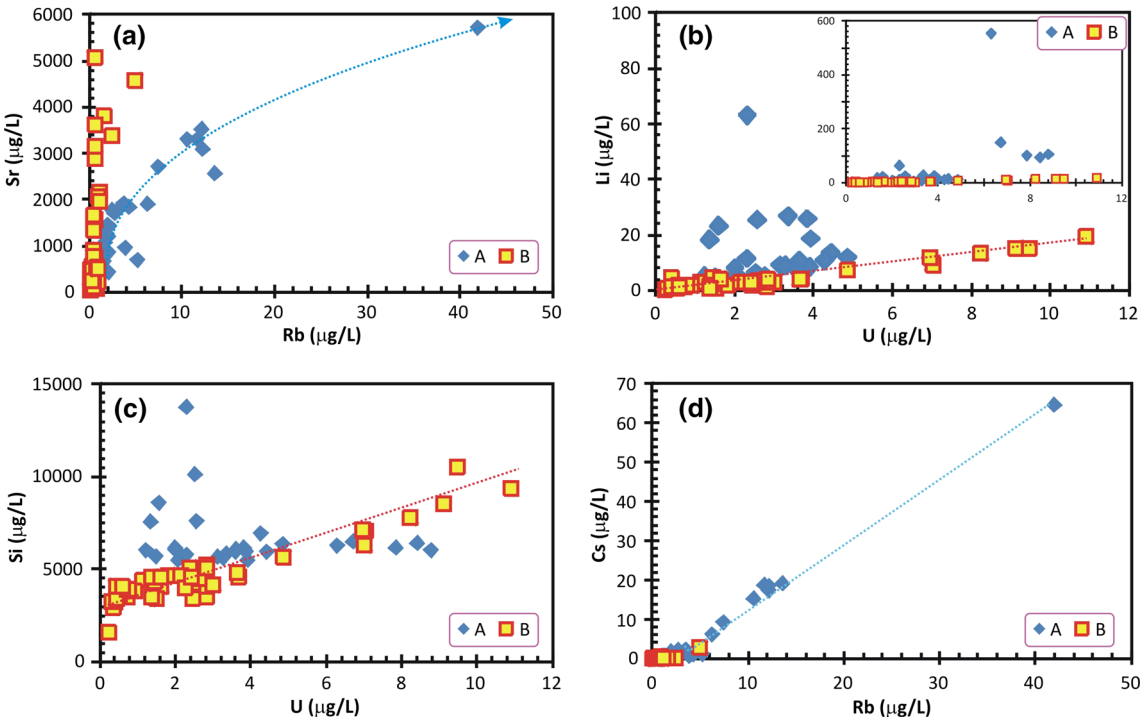

Fig. 6 Hydrochemical relationships between selected minor ions in groundwater. The trend-line of the samples is shown

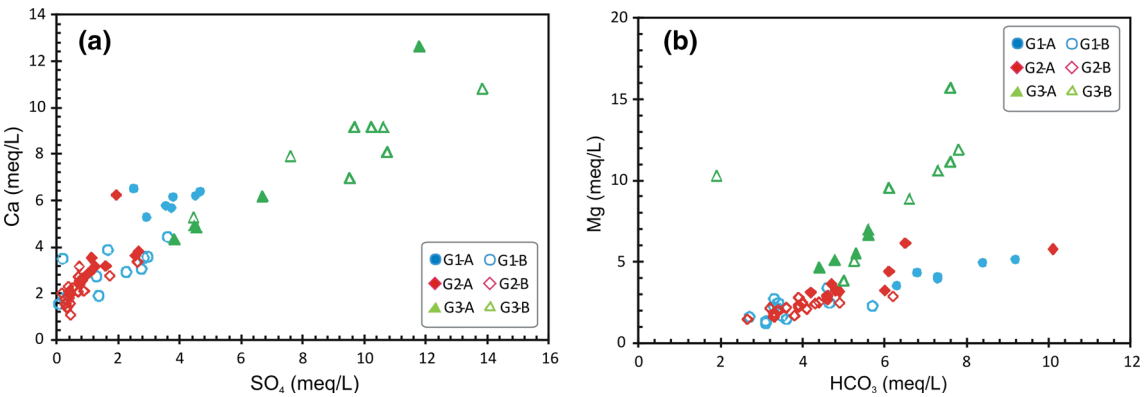

Fig. 7 (**a**) SO_4/Ca and (**b**) HCO_3/Mg ratios. All data are in meq/L. The samples have been classified in groups (G1 to G3) and classes (A and B)

suggested that $\delta^{34}S$ is useful for identifying natural and anthropogenic sources of dissolved sulphate. In the area studied, the $\delta^{34}S$-SO_4 values ranged from −2.8 to 20.6 ‰, while $\delta^{18}O$-SO_4 values ranged between 2.5 and 16.1 ‰ (Fig. 8a; Table 1). According to these data, any direct anthropogenic impact on SO_4 concentrations (sewage, fertilizers) can be excluded. Therefore, the study of the source of the SO_4 focussed on natural sources such as pyrite oxidation and gypsum dissolution. Figure 8a shows the mixing processes affecting $\delta^{34}S$ from gypsum dissolution and sulphide oxidation. The influence of seawater is not significant due to the low percentage of seawater in groundwater samples. Regarding natural sources, the $\delta^{34}S$-SO_4 values of Triassic sulphates are between +15.1 and +16 ‰ for $\delta^{34}S$ and between +10.8 and +16.3 ‰ for $\delta^{18}O$ (Ortí et al. 2014), while the $\delta^{34}S$-SO_4 of sulphides is between +0.4 and +2.6 ‰ for $\delta^{34}S$ and between 0 and +5 ‰ for $\delta^{18}O$ (Arribas and Arribas 1995; García-Lorenzo et al. 2014). The majority of the samples are related to a gypsum dissolution exceeding 40 %. This linear relationship—where the top end is in the region associated with evaporites and the bottom end can be extrapolated into the region associated with sulphide-mineral oxidation—has also been observed at a mining site in an arid climate in the Monument Valley site, Arizona (Miau et al. Miao et al. 2013). Very few of the samples collected (Fig. 8b) lie within the sulphide oxidation field defined by Van Stempvoort and Krouse (1994), which is the zone where the

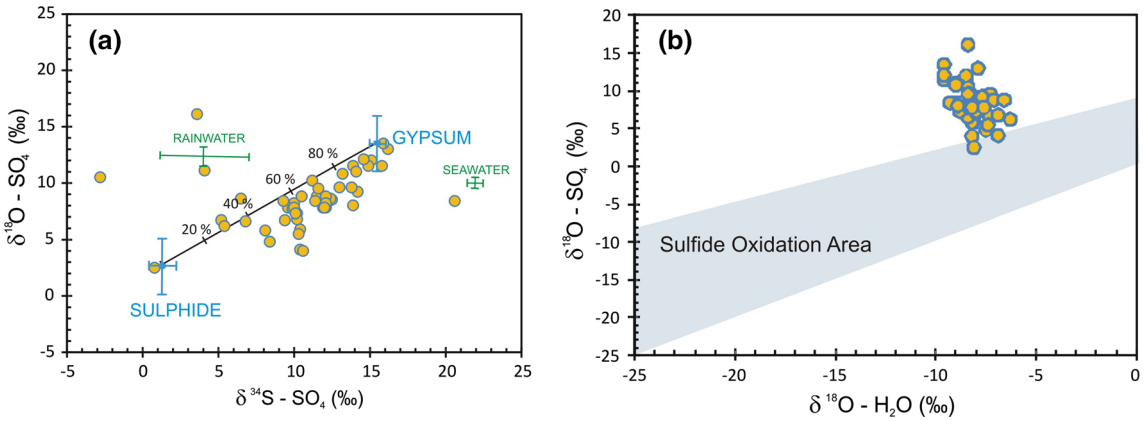

Fig. 8 (**a**) Plot of δ^{34}S-SO_4 versus δ^{34}S-H_2O. Gypsum values are taken from Ortí et al. (2014) and sulphide values from Arribas and Arribas (1995) and García-Lorenzo et al. (2014). Rainwater values are taken from Bottrell et al. (2008) and seawater values from Hosono et al. (2011). (**b**) Plot of δ^{18}O-H_2O versus δ^{18}O-SO_4. The *shaded* area corresponds to the isotopic sulphide oxidation zone defined by Van Stempvoort and Krouse (1994)

isotope data would be plotted if the oxygen of sulphate and water were in isotopic equilibrium. High values of δ^{18}O of sulphate indicate the influence from gypsum/anhydrite dissolution or mixing with such waters.

Tritium and carbon-14 isotopes

Of the 43 samples analysed for ^{3}H, 21 samples contained no ^{3}H above the detection limit of 0.1 TU (Table 1). This indicates these 21 samples are likely to be more than 60 years old. Most of the groundwaters with no measured ^{3}H were from the northern and southern Sierra de Gador. The maximum value was 5.77 TU, indicating that the contribution of rainfall to the groundwater recharge during the last years is very low. Values of >4 TU correspond to areas of klippen and some contact springs on the upper part of the mountain, where groundwater can be considered shallow.

Rb was used to identify the main trends in tritium content, since the concentration of this ion shows a clear relationship with the flowpath and the residence time; thus, samples with short flowpaths have a Rb concentration of around 0 µg/L (class B), whereas the Rb concentration increases in samples corresponding to regional flows (Fig. 6a). Samples classified as A and B according to minor and trace elements were plotted on a graph of Rb vs. tritium (Fig. 9). Most of the samples from class A have low tritium values of less than 1 TU and variable concentrations in Rb. Three samples in this class had tritium concentrations in excess of 1 TU. These samples are affected by marine intrusion (group 4), and, in this case, the tritium content comes from the seawater mixing, which is a recent water (Yechieli et al. 2001; Sivan et al. 2005). Samples belonging to class B have a very low Rb content and variable tritium. However, two groups of samples can be recognized by looking at their tritium concentration. Samples with a concentration of more than 4 TU would come from faster-flowing groundwater flowpaths, while concentrations of less than 3 TU show longer residence times and can be identified with an intermediate flow (Fig. 9).

The ages of the samples were determined using the carbonate dissolution correction-factor calculation proposed by Fontes and Garnier (1979) based on their δ^{13}C and ^{14}C content. This method was selected because it requires the fewest parameter estimates. For calculation purposes, certain values had to be assumed since they were not measured: these included $\delta^{13}C_{CO2} = -17$ ‰, a value obtained for areas with a semiarid climate (Rightmire 1967; Kunkler 1969); $\delta^{13}C_{carb} = 1.4$ ‰, taken from data measured in a carbonate aquifer from northern France (Fontes

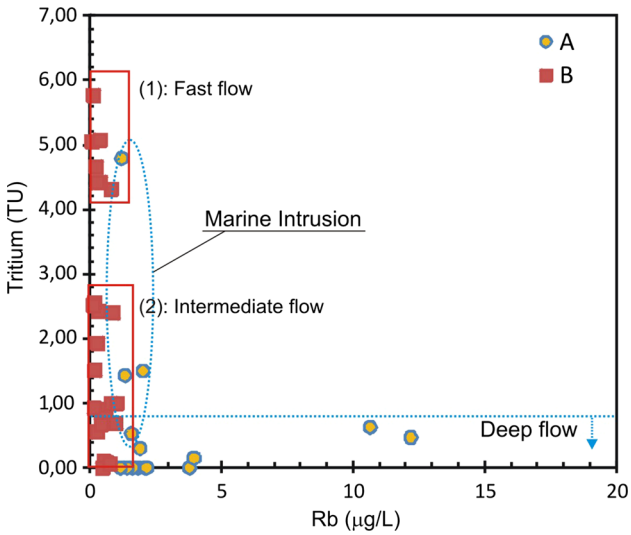

Fig. 9 Rb (µg/L) versus T (TU). The samples have been plotted according to classes A and B

Table 2 Results of isotopic analyses of water samples

Sample	Group	Class	T		$\delta^{34}S$	$\delta^{18}O_{SO4}$	$\delta^{18}O_{H2O}$	^{14}C		$\delta^{13}C$	Age
			TU	±1σ	‰		‰	PMC	±1σ	‰	Ka
1	G4	A									
2	G4	A	1.50	0.09	12	7.8	−7.6	35	0.17	–	M
3	G2-B	A	0.30	0.09	12	8.3	−8.1				
4	G2-B	A	0.00	0.09	9.6	7.8	−8.1				
5	G4	A	0.00	0.09	9.9	7.7	−8.3	10	0.05	−6	7.9
6	G4	A	0.53	0.09							
7	G2-B	B	0.07	0.09	11	4	−8.2				
8	G2-B	A	0.00	0.09	9.4	6.7	−8.2	22	0.11	−7	5.4
9	G2	B									
10	G2	B									
11	G2-B	B			10	5.9	−8.1				
12	G2-B	B	0.10	0.09	8.1	5.8	−8.2				
13	G2-B	B	0.00	0.09	10	7.8	−8.1	42	0.21	−9	3.6
14	G2-B	A	0.00	0.09	5.2	6.7	−8.4				
15	G2-B	B	0.05	0.09	11	8.8	−8.3	28	0.14	−7	1.8
16	G2	A	0.00	0.09							
17	G2	A	0.09	0.09	6.5	8.6	−8.2				
18	G4	B	2.39	0.09							
19	G4	A	0.00	0.09	14	8	−8.9				
20	G3	B	1.00	0.09							
21	G4	A	4.79	0.12				60	0.30	−8	M
22	G1	B	2.43	0.10	8.4	4.8	−7.5				
23	G3	B	5.17	0.12							
24	G2	B	4.31	0.12	12	9.5	−7.3				
25	G2	B	2.51	0.10							
26	G2	B	5.77	0.12	6.8	6.6	−7.3				
27	G4	A	0.15	0.09	5.4	6.2	−6.3	34	0.17	−7	1.0
28	G4	A			12	8.8	−6.6				
29	G1	A			3.6	16.1	−8.4				
30	G1	A			13	8.5	−7.6				
31	G1	A			11	10.2	−8.4				
32	G2	A									
33	G1	A			10	8.2	−8.4				
34	G1	A			4.1	11.1	−8.5				
35	G2-B	B			−2.8	10.5	−8.4				
36	G2-B	A			0.8	2.5	−8.1				
37	G1	B			9.3	8.4	−8.9				
38	G1	A									
39	G1	B			14	11	−9				
40	G1	B	5.05	0.12							
41	G2	B			12	8.2	−8.8				
42	G1	A			14	11.5	−8.6				
43	G2	A			5.6	6.5	−8.4				
44	G3	A			10	7.1	−8				
45	G1	B			10	4.1	−6.9				
46	G1	B	2.56	0.10	16	13	−7.9				
47	G2	B	1.93	0.09							

Table 2 continued

Sample	Group	Class	T		$\delta^{34}S$	$\delta^{18}O_{SO4}$	$\delta^{18}O_{H2O}$	^{14}C		$\delta^{13}C$	Age
			TU	±1σ	‰		‰	PMC	±1σ	‰	Ka
48	G2	A			14	9.2	−7.7				
49	G2	B	1.50	0.09							
50	G1	B	0.90	0.09	16	13.5	−9.6				
51	G1	B	0.92	0.09							
52	G2	B	0.55	0.09							
53	G2	B	0.67	0.09	14	9.6	−8.3				
54	G4	A	1.43	0.09	12	7.8	−8.2	42	0.21	−8	2.1
55	G1	B	0.69	0.09	15	11.5	−9.6				
56	G1	B	0.77	0.09	16	11.5	−9.6				
57	G1	B									
58	G2	B			13	10.8	−9				
59	G2	A									
60	G4	B	0.68	0.09							
61	G1	B			15	12.1	−9.6				
62	G3	B			11	8.4	−9.1				
63	G3	A	0.63	0.09	21	8.4	−9.3				
64	G3	A			12	8.6	−8.4				
65	G3	A			12	8.8	−8.5				
66	G3	A	0.47	0.09	13	9.6	−8.4				
67	G3	B			12	7.8	−8.3				
68	G3	B			10	7.3	−8.8				
69	G3	B			10	5.5	−7.4				
70	G3	B			10	6.8	−6.9				
71	G3	B			10	7.3	−8				
72	G3	B									
73	G3	B	1.00	0.09							
74	G3	A	2.47	0.09	15	12	−8.5				
75	G2	B	5.07	0.12							
76	G2	B	4.66	0.12							
77	G2	B	4.42	0.12							
78	G2	B	4.41	0.12	11	8.8	−7.1				
SW			2.3	0.1			1.06				

Location of sampling points in Fig. 1 (*M*: modern water)

and Garnier 1979); the ^{14}C activity of the soil CO_2 (A_g) was taken as 100 pmC and the ^{14}C activity of solid (A_c) as 0 pmC. Certain values had to be calculated, including the concentration of carbon of inorganic origin from ion balance; the concentration of total dissolved carbon was taken to be that defined by Mook (1976), and the isotope fractionation factor was calculated from Emrich et al. (1970) for the corresponding groundwater temperature.

Using this information, the value of initial ^{14}C activities can be calculated. Substituting these data into the radioactive decay equation yields a mean age for the water samples. The results show that, in general, the waters in the carbonate rocks of the Sierra de Gador are several thousand years old (Tables 1 and 2). The tritium content indicates that, in some cases, this water is mixed with more recent water. They correspond to the sectors closest to the coast, where the effects of sea water intrusion are seen.

Figure 10 shows a conceptual model of the study area, where the relationship between groundwater flow, hydrogeochemical processes and transit time is summarized.

Conclusions

The hydrochemical and isotopic study of the Sierra de Gador aquifer macrosystem has enabled us to recognize a series of processes that explains the chemical differentiation of its waters. The major ion ratios reveal the main

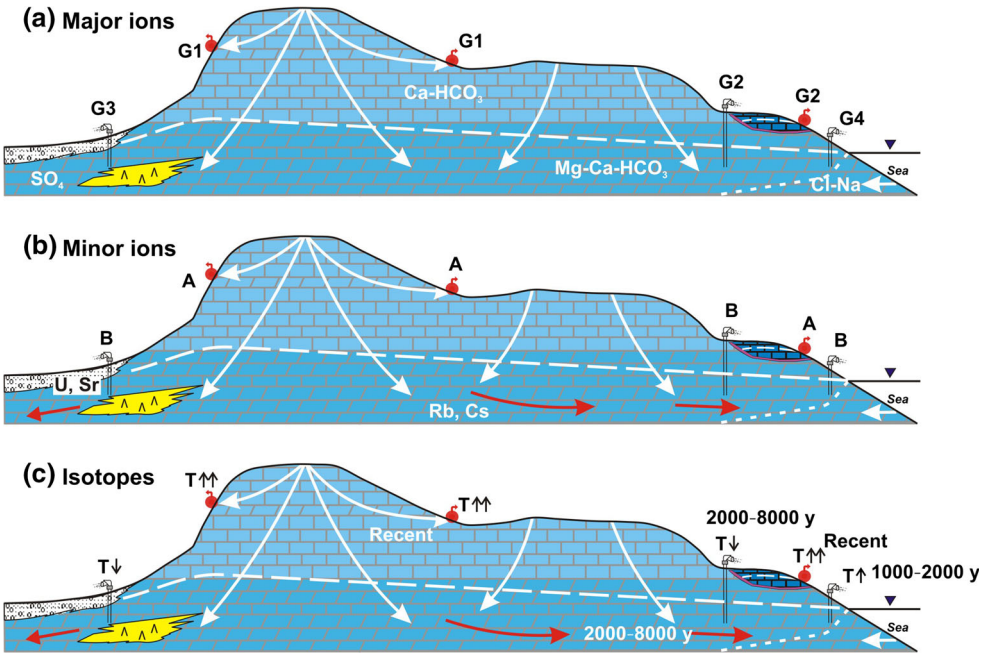

Fig. 10 Scheme of hydrogeochemical processes, groundwater flow and transit time in Sierra de Gádor aquifer system based on (**a**) major ions, (**b**) minor ions and (**c**) isotopes. G1 to G4 correspond to the different established groups, A and B are the defined classes, and T is the tritium content. The groundwater age has also been indicated

causal processes of the mineralization of the waters sampled, classifying them into four groups according to their composition (G1 to G4). These processes are: (1) dissolution of limestone, (2) dissolution of dolomite, (3) dissolution of evaporites, (4) mixing with seawater. Nevertheless, small changes in composition in the minor ions allowed us to recognize some hydrogeochemical processes. The content of Ba and Sr is controlled by sulphate concentration. In the case of Ba, as sulphate increases, so does the SI of the barite, which markedly reduces the barium concentration due to the precipitation of barite. For its part, the Sr concentration of many of the samples was proportional to the sulphate concentration, which is a clear indicator that the Sr forms part of the structure of the gypsum mineralization. Another reason for the increase in certain minor ions is the residence time of water in the aquifer. The samples were classified into two classes (A and B) according to their content in minor ions. Class A corresponded to samples taken from deep boreholes that tapped waters with a long and slow flowpath through the aquifer and which, in some cases, had a higher temperature. Their concentrations of Rb, Cs and U were markedly higher than those in class B. In turn, samples in class B came from springs or shallow boreholes, with shorter residence times. In these, the U/Si ratio showed a linear increase, which indicates that the U comes from the leaching of the detritic deposits.

The study of the radioactive isotopes T and ^{14}C corroborated the apparent residence times of the water in the aquifer. The values of TU in waters in class B generally exceeded 1 TU, indicating a short transit time. On the other hand, class A comprised samples with TUs of less than 1 TU, with the exception of those affected by marine intrusion (in which case the mixing with recent seawater increased the tritium content). The activity of ^{14}C led to estimates of age of between 2 and 8 ky for samples in this class.

Acknowledgments This work takes part of the general research lines promoted by the CEI-MAR Campus of International Excellence as a joint initiative between the universities of Almeria, Granada, Huelva and Málaga, headed by the University of Cádiz. This work was supported by the Andalusia Regional Government, Spain, through the Excellence Research Project P06-RNM-01696 and by MINECO-FEDER, through Project CGL2015-67273-R.

References

Al-Bassam AM, Khalil AR (2012) DurovPwin: a new version to plot the expanded Durov diagram for hydro-chemical data analysis. Comput Geosci 42:1–6

Al-Bassam AM, Awad HS, Al-Alawi JA (1997) DurovPlot a computer program for processing and plotting hydro-chemical data. Groundwater 35(2):362–367

Arribas A, Arribas A (1995) Caracteres metalogénicos y geoquímica isotópica del azufre y el plomo de los yacimientos de minerales metálicos del Sureste de España. Boletín Geológico y Minero 106(1):23–62

Back W, Hanshaw BB, Plummer LN, Rahn PH, Rightmire CT, Rubin M (1983) Process and rate of dedolomitization: mass transfer and ^{14}C dating in a regional carbonate aquifer. Geol Soc Am Bull 94:1415–1429

Barbieri M, Boschetti T, Petitta M, Tallini M (2005) Stable isotope (^{2}H, ^{18}O and $^{87}Sr/^{86}Sr$) and hydrochemistry monitoring for groundwater hydrodynamics analysis in a karst aquifer (Gran Sasso, central Italy). Appl Geochem 20:2063–2081

Bottrell S, Tellam J, Bartlett R, Hughes A (2008) Isotopic composition of sulfate as a tracer of natural and anthropogenic influences on groundwater geochemistry in an urban sandstone aquifer, Birmingham, UK. Appl Geochem 23:2382–2394

Caetano Bicalho C, Batiot-Guilhe C, Seidel JL, Van Exter S, Jourde H (2012) Geochemical evidence of water source characterization and hydrodynamic responses in a karst aquifer. J Hydrol 450–451:206–218

Chiodini G, Frondini F, Marini L (1995) Theoretical geothermometers and pCO_2 indicators for aqueous solution coming from hydrothermal systems of medium-low temperature hosted in carbonate–evaporite rocks. Application to the thermal springs of the Etruscan Swell, Italy. Appl Geochem 10:337–346

Daniele L, Vallejos A, Corbella M, Molina L, Pulido-Bosch A (2013a) Geochemical simulations to assess water–rock interactions in complex carbonate aquifers: the case of Aguadulce (SE Spain). Appl Geochem 29:43–54

Daniele L, Corbella M, Vallejos A, Diaz-Puga M, Pulido-Bosch A (2013b) Geochemical simulations to assess the fluorine origin in Sierra de Gador groundwater. J Geofluids 13(2):221–231

Deike RG (1990) Dolomite dissolution rates and possible Holocene dedolomitization of water-bearing units in the Edwards aquifer, South-Central Texas. J Hydrol 112:335–373

Emrich K, Ehhalt D, Vogel JC (1970) Carbon isotope fractionation during the precipitation of calcium carbonate. Earth Planet Sci Lett 8:363–371

Fontes JC, Garnier JM (1979) Determination of the initial ^{14}C activity of the total dissolved carbon: a review of the existing models and a new approach. Water Resour Res 15(2):399–413

García-Lorenzo ML, Martínez-Sánchez MJ, Pérez-Sirvent C, Agudo I, Recio C (2014) Isotope geochemistry of waters affected by mining activities in Sierra Minera and Portman Bay (SE, Spain). Appl Geochem 51:139–147

Giménez-Forcada E, Vega-Alegre M (2015) Arsenic, barium, strontium and uranium geochemistry and their utility as tracers to characterize groundwaters from the Espadán-Calderona Triassic Domain, Spain. Sci Total Environ 512–513:599–612

Gonfiantini R, Frohlich K, Araguas-Araguas L, Rozanski K (1998) Isotopes in groundwater hydrology. In: Kendall C, McDonnell J (eds) Isotope tracers in catchment hydrology. Elservier, Amsterdam, pp 203–246

Hanor JS (2004) A model for the origin of large carbonate- and evaporite-hosted celestine ($SrSO_4$) deposits. J Sediment Res 74:168–175

Hosono T, Delinom R, Nakano T, Kagabu M, Shimada J (2011) Evolution model of $\delta^{34}S$ and $\delta^{18}O$ in dissolved sulfate in volcanic fan aquifers from recharge to coastal zone and through the Jakarta urban area, Indonesia. Sci Total Environ 409:2541–2554

Krouse HR (1980) Sulphur isotopes in our environment. In: Fritz P, Fontes JC (eds) Isotope geochemistry, vol 1., The terrestrial environmentElsevier, Amsterdam, pp 435–471

Kunkler JF (1969) The sources of carbon dioxide in the zone of aeration of the Bandelier Tuff, near Los Alamos, New Mexico, U.S. Geol. Surv. Prof Pap. 650-B, B 185–B 188

Liesch T, Hinrichsen A, Goldscheider N (2015) Uranium in groundwater—fertilizers versus geogenic sources. Sci Total Environ 536:981–995

Ma R, Wang Y, Sun Z, Zheng C, Ma T, Prommer H (2011) Geochemical evolution of groundwater in carbonate aquifers in Taiyuan, Northern China. Appl Geochem 26(5):884–897

Margat J (2008) Les eaux souterraines dans le monde. Orléans/France, BGRM/UNESCO **187 p**

Martin-Rojas I, Somma R, Delgado F, Estevez A, Iannace A, Perrone V, Zamparelli V (2009) Triassic continental rifting of Pangaea: direct evidence from the Alpujarride carbonates, Betic Cordillera, SE Spain. J Geol Soc 166:447–458

Martín-Rosales W, Gisbert J, Pulido-Bosch A, Vallejos A, Fernández-Cortés A (2007) Estimating groundwater recharge induced by engineering systems in a semiarid area (southeastern Spain). Environ Geol 52:985–995

Martos-Rosillo S, Moral F (2015) Hydrochemical changes due to intensive use of groundwater in the carbonate aquifers of Sierra de Estepa (Seville, Southern Spain). J Hydrol 528:249–263

Miao A, Carroll KC, Brusseau ML (2013) Characterization and quantification of groundwater sulfate sources at a mining site in an arid climate: the monument valley site in Arizona, USA. J Hydrol 504:207–215

Mook WG (1976) The dissolution-exchange model for dating groundwater with 14C. Interpretation of Environmental Isotope and Hydrochemical Data in Groundwater Hydrology. IAEA, Vienna, pp 213–225

Moral F, Cruz-Sanjulián JJ, Olías M (2008) Geochemical evolution of groundwater in the carbonate aquifers of Sierra de Segura (Betic Cordillera, southern Spain). J Hydrol 360:281–296

Morgantini N, Frondini F, Cardellini C (2009) Natural trace elements baselines and dissolved loads in groundwater from carbonate aquifers of central Italy. Phys Chem Earth 34:520–529

Ortí F, Pérez-López A, García-Veigas J, Rosell L, Cendón DI, Pérez-Valera F (2014) Sulfate isotope compositions ($\delta^{34}S$, $\delta^{18}O$) and strontium isotopic ratios ($^{87}Sr/^{86}Sr$) of Triassic evaporates in the Betic cordillera (SE Spain). Rev Soc Geol Esp 27(1):79–90

Parkhurst DL, Appelo CAJ (2013) Description of input and examples for PHREEQC version 3–A computer program for speciation, batch- reaction, one-dimensional transport, and inverse geochemical calculations: U.S. Geological Survey Techniques and Methods, book 6, chap. A43

Plummer LN (2005) Dating of young groundwater. Isotopes in the water cycle. Springer, Dordrecht, pp 193–218

Reynauld A, Guglielmi J, Mudry J, Mangan C (1999) Hydrochemical approach to the alteration of the recharge of a karst aquifer consecutive to a long pumping period: example taken from Pinchinade Graben (Mouans-Sartoux, French Riviera). Groundwater 37:414–417

Rightmire CT (1967) A radiocarbon study of the age and origin of caliche deposits. M.A. thesis, University of Texas, Department of Geology Science, Austin

Rodríguez-Fernández J, Martín-Penela AJ (1993) Neogene evolution of the Campo de Dalias and surrounding off-shore areas (Northeastern Alboran Sea). Geodin Acta 6:255–270

Sánchez D, Barberá JA, Mudarra M, Andreo B (2015) Hydrogeochemical tools applied to the study of carbonate aquifers: examples from some karst systems of Southern Spain. Environ Earth Sci 74:199–215

Sanz de Galdeano C, Rodriguez-Fernández J, López-Garrido AC (1985) A strike-slip fault corridor within the Alpujarra mountains (Betic Cordilleras, Spain). Geol Rundsch 74:641–655

Saunders JA, Toran LE (1994) Evidence for dedolomitization and mixing in paleozoic carbonates near Oak Ridge, Tennessee. Gr Water 32(2):207–214

Sdao F, Parisi S, Kalisperi D, Pascale S, Soupios P, Lydakis-Simantiris N, Kouli M (2012) Geochemistry and quality of the groundwater from the karstic and coastal aquifer of geropotamos river basin at north-central Crete, Greece. Environ Earth Sci 67:1145–1153

Sivan O, Yechieli Y, Herut B, Lazar B (2005) Geochemical evolution and timescale of seawater intrusion into the coastal aquifer of Israel. Geochim Cosmochim Acta 69:579–592

Stamatakis MG, Tziritis EP, Evelpidou N (2009) The geochemistry of Boron-rich groundwater of the Karlovassi Basin, Samos Island, Greece. Cent Eur J Geosci 1(2):207–218

Terzić J, Marković T, Pekaš Ž (2008) Influence of sea-water intrusion and agricultural production on the Blato Aquifer, Island of Korčula, Croatia. Environ Geol 54:719–729

Underwood EC, Ferguson GA, Betcher R, Phipps G (2009) Elevated Ba concentrations in a sandstone aquifer. J Hydrol 376:126–131

Valentino GM, Stanzione D (2003) Source processes of the thermal waters from the Phlegraean Fields (Naples, Italy) by means of the study of selected minor and trace elements distribution. Chem Geol 195:245–274

Vallejos A, Andreu JM, Sola F, Pulido-Bosch A (2015a) The anthropogenic impact on Mediterranean karst aquifers: cases of some Spanish aquifers. Environ Earth Sci 74:185–198

Vallejos A, Díaz-Puga MA, Sola F, Daniele L, Pulido-Bosch A (2015b) Using ion and isotope characterization to delimitate a hydrogeological macrosystem. Sierra de Gador (SE, Spain). J Geochem Explor 155:14–25

Van Stempvoort DR, Krouse HR (1994) Controls of $\delta^{18}O$ in sulfate—Review of experimental data and application to specific environments, In: Alpers CN, Blowes DW (eds) Environmental geochemistry of sulfide oxidation: American Chemical Society Symposium Series 550, 446–480

Vengosh A, Spivack AJ, Artzi Y, Ayalon A (1999) Geochemical and boron, strontium, and oxygen isotopic constraints on the origin of the salinity in groundwater from the Mediterranean coast of Israel. Water Resour Res 35:1877–1894

Wu P, Tang C, Zhu L, Liu C, Cha X, Tao X (2009) Hydrogeochemical characteristics of surface water and groundwater in the karst basin, southwest China. Hydrol Process 23(14):2012–2022

Xanke J, Goeppert N, Sawarieh A, Liesch T, Kinger J, Ali W, Hötzl H, Hadidi K, Goldscheider N (2015) Impact of managed aquifer recharge on the chemical and isotopic composition of a karst aquifer, Wala reservoir, Jordan. Hydrogeol J 23:1027–1040

Yechieli Y, Sivan O, Lazar B, Vengosh A, Ronen D, Herut B (2001) Radiocarbon in seawater intruding into the Israeli Mediterranean coastal aquifer. Radiocarbon 43:773–781